Protein Engineering, Design & Selection, 2018, vol. 31 no. 5, pp. 159–171
doi: 10.1093/protein/gzy013
Advance Access Publication Date: 21 June 2018
Original Article

OXFORD

Original Article

Adnectin–drug conjugates for Glypican-3-specific delivery of a cytotoxic payload to tumors

Daša Lipovšek[1,*], Irvith Carvajal[1], Alban J. Allentoff[2], Anthony Barros Jr.[3], John Brailsford[2], Qiang Cong[4], Pete Cotter[1], Sanjeev Gangwar[4], Cris Hollander[1], Virginie Lafont[5], Wai Leung Lau[1], Wenying Li[3], Miguel Moreta[1], Steven O'Neil[1], Jason Pinckney[1], Michael J. Smith[6], Julie Su[1], Christina Terragni[1], Michael A. Wallace[2], Lifei Wang[3], Martin Wright[1], H. Nicholas Marsh[1], and James W. Bryson[1]

[1]Molecular Discovery Technologies, Bristol-Myers Squibb, Waltham, MA 02453, USA, [2]Radiochemistry, Bristol-Myers Squibb, Lawrenceville, NJ 08648, USA, [3]Preclinical Candidate Optimization, Bristol-Myers Squibb, Lawrenceville, NJ 08648, USA, [4]Discovery Chemistry Oncology, Bristol-Myers Squibb, Redwood City, CA 94063, USA, [5]Molecular Discovery Technologies, Bristol-Myers Squibb, Lawrenceville, NJ 08648, USA, and [6]Chemical and Synthetic Development, Bristol-Myers Squibb, New Brunswick, NJ 08903, USA

[*]To whom correspondence should be addressed. E-mail: dasa.lipovsek@bms.com
Edited by E.M. Meiering

Received 27 March 2018; Revised 21 May 2018; Editorial Decision 27 May 2018; Accepted 30 May 2018

Abstract

Tumor-specific delivery of cytotoxic agents remains a challenge in cancer therapy. Antibody–drug conjugates (ADC) deliver their payloads to tumor cells that overexpress specific tumor-associated antigens—but the multi-day half-life of ADC leads to high exposure even of normal, antigen-free, tissues and thus contributes to dose-limiting toxicity. Here, we present Adnectin–drug conjugates, an alternative platform for tumor-specific delivery of cytotoxic payloads. Due to their small size (10 kDa), renal filtration eliminates Adnectins from the bloodstream within minutes to hours, ensuring low exposure to normal tissues. We used an engineered cysteine to conjugate an Adnectin that binds Glypican-3, a membrane protein overexpressed in hepatocellular carcinoma, to a cytotoxic derivative of tubulysin, with the drug-to-Adnectin ratio of 1. We demonstrate specific, nanomolar binding of this Adnectin–drug conjugate to human and murine Glypican-3; its high thermostability; its localization to target-expressing tumor cells *in vitro* and *in vivo*, its fast clearance from normal tissues and its efficacy against Glypican-3-positive mouse xenograft models.

Key words: Adnectin, Adnectin–drug conjugate, Glypican-3, hepatocellular carcinoma, tubulysin

Introduction

The high affinity and exquisite specificity of natural antibodies gave rise to the earliest ideas of using antibodies as 'magic bullets', which would deliver a highly potent compound to the exact tissue where it is needed, yet would minimize exposure to other tissues (Strebhardt and Ullrich, 2008). The advances in monoclonal antibody and antibody humanization technologies cleared the path to the development of antibody–drug conjugates (ADC), which were designed to

deliver powerful chemotherapy agents to tumors targeted by the antibody. Once a cancer cell internalizes the ADC bound to its surface antigen, the cytotoxic agent is released inside the cell, causing cell death (Sievers and Senter, 2013).

The first FDA-approved ADC was Mylotarg (gentuzumab ozogamicin), which targets the tumor-associated antigen CD33, for the treatment of acute myeloid leukemia (Bross *et al.*, 2001). In the 17 years that spanned the original approval of Mylotarg, its withdrawal from the market due to poor safety and clinical benefit and its re-approval (at a lower dose and for a different patient population) (Appelbaum and Bernstein, 2017), more than 60 ADC molecules have entered clinical trials, but only three more have been approved so far: (i) Adcetris (brentuximab vedotin), which targets CD30, for Hodgkin lymphoma and anaplastic large cell lymphoma (Younes *et al.*, 2010); (ii) Kadcyla (trastuzumab emtansine), which targets HER2, for breast cancer (Verma *et al.*, 2012) and (iii) Besponsa (inotuzumab ozogamicin), which targets CD22, for B-cell precursor acute lymphoblastic leukemia (Lamb, 2017).

The relatively low success rate of new ADC drugs reflects the disappointing reality that, whereas many of these drugs do deliver their cytotoxic payload to tumors that overexpress their target, they also deliver significant amounts of the cytotoxic payload to normal tissues, leading to dose-limiting toxicity and a low ratio of efficacy to toxicity (therapeutic index) (Saber and Leighton, 2015). The excessive toxicity of ADC is likely to be due to a combination of 'off-tumor, on-target toxicity', where the ADC delivers its payload to a normal tissue that expresses some of the antigen the antibody was raised against, and 'off-target toxicity', where the ADC delivers the toxic payload to a normal tissue that does not express the target. Off-tumor, on-target toxicity can be minimized by judicious selection of a target with the highest possible ratio in expression level on cancer vs. normal cells. In contrast, off-target toxicity, where the ADC is internalized by cells that do not express its target, by either non-specific pinocytosis or through an Fc or mannose receptor-directed mechanism, has been difficult to combat. This difficulty is a consequence of the multi-day ADC half-life in the bloodstream: while only a small fraction of an injected ADC localizes to the tumor, the remaining ADC circulates in the bloodstream for several days to over a week, feeding the non-specific uptake and catabolism pathways and killing those normal cells that internalize it. The view that off-target mechanisms are the dominant contributors to ADC toxicity (Polakis, 2015) is supported by the observation that toxicity profiles are more similar for ADC that target different antigens but deliver the same cytotoxic payload than for ADC that target the same antigen but deliver cytotoxic payloads with different modes of action (Saber and Leighton, 2015; Donaghy, 2016).

To date, approaches to reducing ADC off-target toxicity have focused on improving ADC homogeneity and biophysical properties through site-directed conjugation (Strop *et al.*, 2013, 2015); on controlling the stability of linkers between the antibody and the payload (Polakis, 2015) and on making the binding to the target antigen or the release of the cytotoxic payload conditional on tumor microenvironment (Joubert *et al.*, 2017). Whereas these approaches are likely to mitigate any off-target toxicity due to cellular uptake of aggregation-prone, over-conjugated ADC, and due to premature release of cytotoxic payload, these approaches are unlikely to address the problem of non-specific or Fc receptor-mediated internalization of circulating ADC by normal cells.

In contrast, our approach to reducing off-target toxicity is to limit exposure of normal tissues to the cytotoxic payload. To achieve this, we employ a family of targeting proteins that have an extremely short half-life in the bloodstream and that do not bind Fc receptors or other receptors involved with protein uptake by normal cells. These engineered targeting proteins are Adnectins (Koide *et al.*, 1998, Lipovšek, 2010), single-domain derivatives of the 10th human fibronectin type III domain (Main *et al.*, 1992, Dickinson *et al.*, 1994), which can be selected from complex libraries using *in vitro* methods. Due to their small size (10 kDa for an Adnectin and 12 kDa for an Adnectin–drug conjugate), these molecules are eliminated from the bloodstream through fast, mechanical filtration by the kidney (Lin, 2009), with the half-life in the bloodstream in the range of 20–30 min in rodents and 1–2 h in cynomologous monkeys and humans. In contrast to catabolism in the liver, which is the elimination pathway for ADC, renal filtration does not involve cellular uptake of the protein being eliminated; this reduces the risk of release of the toxic payload and of resulting toxicity. We find that, despite their fast clearance, Adnectin–drug conjugates can localize to tumors that overexpress their target and show a robust efficacy in mouse xenograft models.

Conjugates and genetic fusions between small, engineered, non-antibody domains that bind tumor-associated targets and cytotoxic payloads have been described previously (Martin-Killias *et al.*, 2011; Simon *et al.*, 2013; Cox *et al.*, 2016; Currier *et al.*, 2016; Goldberg *et al.*, 2016; Sochaj-Gregorczyk *et al.*, 2016, 2017; Serwotka-Suszczak *et al.*, 2017; Sokolova *et al.*, 2017). In contrast to the conjugates described here, the majority of the previously reported scaffold–drug conjugates that have been tested in animal models had been modified to extend their naturally short half-life to approximate the pharmacokinetics of antibodies, with the goal of maximizing exposure of tumors to the cytotoxic payloads and thus maximizing efficacy. Such modifications have included chemical conjugation to albumin (Simon *et al.*, 2014) and genetic fusion to Fc (Currier *et al.*, 2016). We speculate that scaffold–drug conjugates with antibody-like pharmacokinetic properties are likely to encounter dose-limiting toxicity similar to that of ADC. In contrast, we propose that fast-clearing drug conjugates with small (<50 kDa), high-affinity and biophysically robust scaffolds are likely to maximize the ratio of cytotoxic payload delivered to the tumor over that delivered to target-free normal tissues, i.e. the ratio of efficacy over off-target toxicity. This prediction is supported by the biodistribution pattern of radiolabeled, HER2-binding ankyrin repeat proteins (DARPINs; without cytotoxic payloads) that were either left unmodified or were conjugated to 20-kDa polyethylene glycol (PEG) (Zahnd *et al.*, 2010). After 2 days, a similar amount of the two DARPINs was found in xenografted tumors, but an order of magnitude more PEGylated than unmodified DARPIN was still present in the blood.

Our scaffold proteins of choice, Adnectins, bear a superficial structural similarity to a single variable domain of an antibody (Fig. 1A) but do not share a significant sequence homology with antibodies and do not contain a cross-beta-sheet disulfide found in natural antibody domains, or any other cysteines. As a consequence, a single exposed cysteine can be engineered into an Adnectin to serve as the site for site-specific conjugation, e.g. using maleimide chemistry. In the past Adnectin-therapeutic candidates, such specific conjugation has been used to modify Adnectin C-termini with PEG for a larger hydrodynamic radius and longer half-life (Tolcher *et al.*, 2011; Mitchell *et al.*, 2014). In the application described here, site-directed conjugation is used to construct covalent conjugates (Fig. 1A) between an Adnectin and a payload (Fig. 1B), which in turn consists of a cathepsin-B-cleavable dipeptide linker (Dubowchik *et al.*, 2002) and a cytotoxic small molecule, an analog

of tubulysin (Murray *et al.*, 2015). The tubulysin analog inhibits microtubule formation and thus is highly toxic to dividing cells, including cancer cells, when delivered intracellularly. Due to the single C-terminal cysteine in the engineered Adnectin and to the high efficiency and specificity of maleimide chemistry, the drug-to-Adnectin ratio in the conjugates (DAR) is 1.0.

The target of the Adnectin–drug conjugates described in this study is human Glypican-3, a membrane protein overexpressed in hepatocellular carcinoma and associated with poor prognosis (Filmus and Capurro, 2013; Haruyama and Kataoka, 2016). Glypican-3-binding antibodies are being pursued as possible therapeutics, both as unmodified antibodies (Zhu *et al.*, 2013, Ikeda *et al.*, 2014) and as targeting domains of immunotoxins (Fleming and Ho, 2016) and of T-cell-activating bispecific antibodies (Ishiguro *et al.*, 2017).

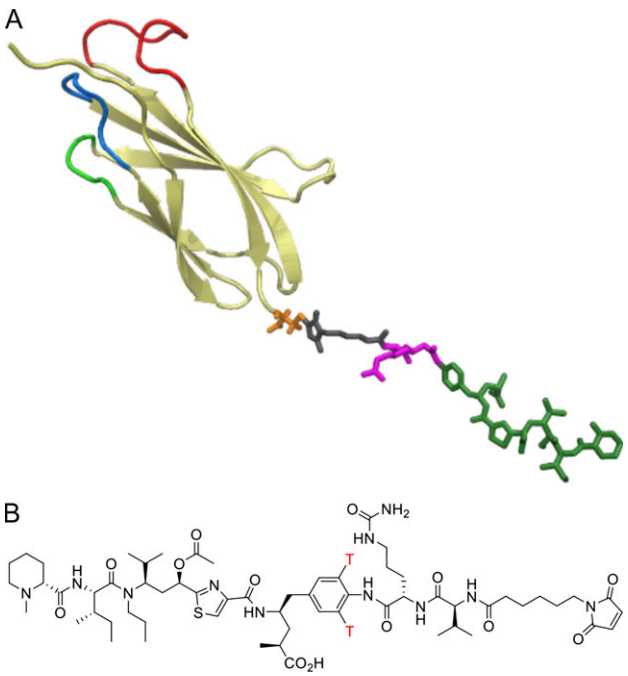

Fig. 1 Molecular models of Adnectin–drug conjugate and its small-molecule payload (linker and tubulysin analog). (**A**) Molecular model of A-RGE-tub (non-binding control) Adnectin—drug conjugate. Yellow ribbon: backbone with sequence identical between wild-type 10Fn3, A-RGE and Glypican-3-binding Adnectins A0, A1 and A2. Blue: backbone of loop BC. Light green: backbone of loop DE. Red: backbone of loop FG. Orange: side chain of C-terminal cysteine. Gray: maleimide and spacer. Magenta: valine–citrulline, cleavable linker. Dark green: tubulysin analog. The model was constructed based on crystal structures of wild-type 10Fn3 (1FNA) and of the tubulysin analog. (**B**) Molecular structure of the linker and tubulysin analog. T: hydrogen atoms substituted with tritium in the Adnectin–drug conjugate used for quantitative whole body autoradiography (Fig. 3).

Materials and Methods

Preparation of recombinant Glypican-3

The extracellular domain of human Glypican-3 protein, fused at its C-terminus to a portion of human IgG1 (Supplementary Table SI), was cloned in a pTT vector, and expressed following a published protocol (Durocher *et al.*, 2002). HEK293-6E cells at 1×10^6 cells/ml were transfected with the vector, using a 1:2 DNA:PEI (polyethylenimine) ratio. Four liters of conditioned media were harvested by sedimentation 5 days post-transfection and filtered through 0.45-μm filters. The cell density at harvest was approximately 2.2×10^6 cells/ml, and the cell viability was approximately 74%.

The conditioned medium was loaded onto a 5-ml MabSelect SuRe column (GE Healthcare). The column was washed with PBS, pH 7.4 (Cellgro), then with PBS, 0.5 M Arginine (contact time of 30 min), followed by a final wash with PBS. The protein was eluted from the column with 100 mM Glycine, pH 2. The eluted fractions were collected into tubes containing 20% of the final volume of 1 M Tris, pH 9. The fractions eluted from the MabSelect SuRe column were pooled and loaded onto a Superdex 200 HiLoad 26/60 (GE Healthcare) pre-equilibrated with PBS, pH 7.4. The fractions containing the protein were pooled and concentrated to 1 mg/ml.

The fusion between the extracellular domain of murine Glypican-3 and human IgG1 (mGPC3-hIgG1) was purchased from R&D Systems. Both hGPC3-hIgG1 and mGPC3-hIgG1, at 1 mg/mL in PBS, were biotinylated using EZ-link Sulfo-NHS Biotin (Pierce) at 20× molar excess. The reaction was incubated at room temperature for 1 h, then dialyzed in a Slide-A-Lyzer, 3.5 K MWCO, dialysis cassette (Thermo Scientific), against PBS, for 1 h, then overnight using fresh buffer. Aliquots were stored at −80°C.

Discovery of Glypican-3-binding Adnectins

Glypican-3-binding Adnectins were selected, using mRNA display, from ^{10}Fn3-based libraries in which sequence and length of loops BC, DE and FG were diversified to the complexity of 5.3×10^{13} (Table I). The selection method followed had been described

Table I. CDR-like loops, C-termini and chemical modifications of Glypican-3-binding and control Adnectins

Adnectin ID	Loop BC	Loop DE	Loop FG—Strand G	C-terminus	Modification on Cys
^{10}Fn3	DAPAVTV	GSKS	GRGDSPASSK—P	NYRT	No Cys
A-RGE-alk	DAPAVTV	GSKS	GRGESPASSK—P	NYRTPC	Alkylated
A-RGE-tub	DAPAVTV	GSKS	GRGESPASSK—P	NYRTPC	Tubulysin analog
A-RGE-H-tub	DAPAVTV	GSKS	GRGESPASSK—P	NYRTPCHHHHHH	Tubulysin analog
Naïve library	XXXXXXX	XXXX	XXXXXXXXXX—P	NYRT	
A0H	SGDYHPH	GEHE	YDGEKADKYP—P	NYRTEID KPSQHHHHHH	No Cys
Affinity maturation library	sgdYhph	geHe	Ydgekadkyp—P	NYRT	No Cys
A1-alk	SDDYHAH	GEHV	YDGEKAATDW—S	NYRTPC	Alkylated
A1-tub	SDDYHAH	GEHV	YDGEKAATDW—S	NYRTPC	Tubulysin analog
A1H-tub	SDDYHAH	GEHV	YDGEKAATDW—S	NYRTPCHHHHHH	Tubulysin analog
A2-alk	SDDYHAH	GEHV	YDAEKAATDW—S	NYRTPC	Alkylated
A2-tub	SDDYHAH	GEHV	YDAEKAATDW—S	NYRTPC	Tubulysin analog

X—any amino acid residue except for Cys and Met. Lower-case letter: 50% probability of the named amino acid residue; 50% probability of a different amino acid residue. Underlined: selected amino acid residues that are different from the corresponding residues in A0H.

previously (Xu *et al.*, 2003), except for two protocol modifications: first, the mRNA library was ligated to the puromycin linker (5′ C6-Psoralen-UAGCGGAUGC-PEG-dCdC-Puromycin-3′, Glen Research) using UV-mediated cross-linking (Kurz *et al.*, 2000). Second, selection progress was followed using quantitative PCR with an intercalating dye (SYBR Green, Thermofisher) and a pair of primers complementary to the constant regions of the ^{10}*Fn3* gene.

During each of the three rounds of mRNA display selection from the naïve library, populations of Adnectin–mRNA fusions annealed to their complementary DNA were incubated with 100 nM human Glypican-3–Fc for 30 min at room temperature. Incubation volumes were 400 µl in round 1, 300 µl in round 2 and 100 µl in round 3 and later rounds. Adnectin–mRNA fusions were then captured with an equal volume of protein-G-coated magnetic beads (ThermoFisher). The cDNA encoding the captured library members was amplified by PCR and served as an input for the next round of selection. In rounds 2 and 3, each Adnectin–mRNA/cDNA population was incubated with 100 nM Fc, and the flow-through retained, three times in a row before applying the positive selection against human Glypican-3–Fc.

The enriched population of approximately 1.5×10^4 *Adnectin* genes recovered from round 3 of mRNA display selection were transferred into yeast surface display. In the yeast display system supplied by BAC B.V., the BioAffinity Company (Naarden, Netherlands), each clone of interest is expressed as a genetic fusion with a secretion signal sequence at the N-terminus, and with α-agglutinin 1 (US Patent 6114147), a yeast cell wall surface glycoprotein, at the C-terminus (Supplementary Fig. S1A and B).

The yeast display vector used in this study, pDV-23, was derived from the BioAffinity Company vector pBYD02 by replacing the fragment between XhoI and SpeI restriction sites with DNA encoding wild-type ^{10}Fn3 N- and C-termini, separated by a spacer with multiple NcoI and NdeI restriction sites. The full sequence of plasmid pDV-23 is shown in Supplementary Fig. S1C.

To incorporate the Adnectin clones enriched by mRNA display into pDV-23, the DNA population was PCR-amplified with primers complementary to the plasmid pDV-23. Four microgram of the amplified DNA encoding the Adnectin population and 4 µg of linearized pDV-23 were then co-electroporated (Benatuil *et al.*, 2010) into 6.4×10^7 yeast cells of strain VWK18gal-, resulting in a library of Adnectins under control of GAL7 promoter and fused, through their C-termini, to c-myc epitope, and to the gene encoding α-agglutinin 1.

During each of the subsequent four rounds of yeast surface display, the yeast harboring the Adnectin gene population were inoculated into media YSD (20 g/l glucose, 6.7 g/l yeast nitrogen base with ammonium sulfate, 1.6 g/l yeast synthetic drop out media supplements without leucine (Sigma Y1376)), at the cell density of 0.2 OD, and grown at 30°C, 220 rpm, until they reached the cell density of 1–2 OD. The culture was then pelleted by centrifugation, resuspended in YPG (10 g/l of Bacto Yeast extract, 20 g/l of BactoPeptone, 20 g/l of galactose) at the cell density of 0.1 OD and grown at 30°C, 220 rpm, for 16–20 h. Induced yeast cells were pelleted, washed using PBS, 0.1% (*w/v*) bovine serum albumin, and labeled, as described previously (Lipovšek *et al.*, 2007). The number of induced cells labeled in rounds 1, 2, 3 and 4 was 2×10^8, 5×10^7, 5×10^6 and 5×10^6, respectively. To visualize each Adnectin displayed on the yeast surface, the C-terminal epitope tag was labeled using an anti-c-myc primary antibody and a secondary, fluorescently labeled antibody. The primary/secondary antibody combination used in rounds 1 and 3 was chicken-anti-c-myc (Invitrogen A-21281) and goat-anti-chicken-A633 (Invitrogen A-21103); and the combination used in rounds 2 and 4 was mouse-anti-c-myc 9E10 (Covance MMS-150R) and goat-anti-mouse-A633 (Invitrogen A-21052).

To visualize the Adnectins that were capable of binding Glypican-3, the population was incubated with 100 nM biotinylated human Glypican-3 (R&D Systems, 2119-GP-050/CF), followed by anti-biotin detection. Rounds 1 and 3 used Streptavidin-A488 (Invitrogen S-32354), and rounds 2 and 4 used goat-anti-biotin-DyLight488 antibody (Rockland 600-141-098). Fluorescence-activated cell sorter BD FACSAria II was used to capture the yeast cells with the optimal combination of display and binding signal. The captured yeast population was allowed to regrow, then was re-induced, re-labeled and re-sorted. The fraction of the yeast population with positive signal for both display and Glyipican-3 binding in rounds 1–4 was approximately 7.7, 7.1, 14 and 10%. The subset of this population with the strongest display level (i.e. the largest number of Adnectin molecules displayed per yeast cell) was collected, increasing the stringency of gating with each round. The fraction of yeast population captured in rounds 1–4 was 2.6, 0.5, 0.5 and 0.15%. Plasmids containing the genes of enriched Adnectins were recovered from the post-round-4 yeast population (in the 0.15% gate) using Zymoprep Yeast Plasmid Miniprep Kit II (Zymo Research D2004). The Adnectin genes were subcloned into plasmid pET9d, sequenced, then expressed and screened in 96-plate format (Koide *et al.*, 2012).

The Adnectin with the most favorable properties, A0 (Table I, Supplementary Table SI), was affinity-matured by re-diversifying the sequences of its selected loops BC, DE and FG. Each nucleotide in a re-diversified loop was replaced with a mixture of nucleotides, with 70% of the mix containing the selected nucleotide, and the remaining 30% comprising 10% each of the remaining three nucleotides. The resulting, affinity maturation, library was subjected to selection by mRNA display similar to the selection described above but under more stringent conditions. Concentration of human Glypican-3–Fc during affinity maturation rounds 1 and 2 was 100 nM and 10 nM, respectively. Rounds 3–7 were performed using 10 nM biotinylated human Glypican-3–Fc, with an increasing stringency for the rate of dissociation from the target: after the 30-min incubation with the biotinylated Glypican-3–Fc, 100× excess (1 µM) unbiotinylated human Glypican-3–Fc was added. In affinity maturation rounds 4, 5, 6 and 7, the competition between biotinylated and unbiotinylated targets was allowed to proceed for 30 min, 3, 5, 7 and 15 h, respectively. The competition was stopped by the addition of Dynabeads streptavidin beads (ThermoFisher). The Adnectin–mRNA/cDNA molecules that were captured on streptavidin beads after the 15-h incubation in round 7 were PCR-amplified, cloned, expressed in *Escherichia coli* and screened for binding to Glypican-3 and for robust biophysical properties (Koide, Koide and Lipovšek, 2012). The clone with the most desirable combination of properties was further mutated to introduce a proline and a cysteine into its C-terminus, resulting in Adnectin A1 (Table I, Supplementary Table SI). We then replaced the Asp-Gly dipeptide in the A1 FG loop with the Asp-Ala dipeptide, to generate the lead Adnectin, A2 (Table I, Supplementary Table SI). (The Asp-Ala dipeptide was chosen after a survey of properties of Adnectins with eight different amino acid substitutions in the Asp-Gly dipeptide (data not shown).)

Preparation of Adnectin–drug conjugates

Each gene encoding an Adnectin of interest was cloned into vector pET9d (Novagen) and transformed into the BL21 (DE3) pLysS strain of *E. coli* (Novagen).

The hexahistidine-tagged Adnectins, A0H, A1H and A-RGE-H, were expressed and purified using a standard published protocol (Mamluk *et al.*, 2010).

For the untagged Adnectins, A1 and A2, a starter culture was grown to absorbance at 600 nm (A_{600}) of 1.0 in a shake flask containing LB, 100 mg/l kanamycin, at 25°C, 250 rpm, then used to inoculate a 10-l fermentor (Sartorius) containing 8 L of Complex Media (15 g/l yeast extract (EMD), 30 g/l BBL phytone peptone (BD), 0.1 g/l ferric ammonium citrate (J.T. Baker), 1.9 g/l citric acid (Mallinckrodt), 2.1 g/l ammonium chloride (Mallinckrodt), 1.38 g/l monobasic sodium phosphate (J.T. Baker), 10 g/l glycerol (EMD), 20 g/l dextrose (Mallinckrodt), 0.385 g/l magnesium sulfate (J.T. Baker), 100 mg/l kanamycin (Amresco), adjusted to pH 6.85 with ammonium hydroxide (Mallinckrodt)). The starting A_{600} was 0.003. The fermentation was first maintained at 25°C, one vessel volume per minute air, for 17 h, maintaining a 30% dissolved oxygen level by increasing the impeller speed from 250 to 800 rpm, then by increasing oxygen flow. After 17 h, temperature was increased to 37°C. When the culture reached A_{600} of 22, the fermentor temperature was reduced to 30°C. When the culture reached A_{600} of 25, the culture was induced by adding 1 mM isopropyl-ð½-D-thiogalactopyranoside (IPTG), and a 5 ml/min feed (30 g/l yeast extract, 60 g/l phytone peptone, 100 g/l glycerol, 100 mg/l kanamycin, pH 6.85) was initiated. The fermentor was harvested 4 h after induction. The media were centrifuged at 15 000 × *g* for 30 min, and the cell paste was frozen at −80°C.

The cell paste was homogenized in 10× volume/mass lysis buffer (20 mM phosphate, pH 6.8, 0.3 M NaCl,10 mM EDTA), using an Ultraturrax T18, at speed 2, for 30 min. The cells were lysed using two passes at 15 000 psi through Microfluidizer M110EH, and debris was removed by centrifugation at 15 000 × *g* for 30 min. The supernatant was diluted with a 4× volume of 100 mM glycine, pH 3.0, for a final pH of 3.5, incubated for 1 h at room temperature and filtered using an Acropak 1000 capsule (Pall). The sample was loaded onto an SP Sepharose, fast-flow cation-exchange column (GE Healthcare), pre-equilibrated with three column volumes of 50 mM acetate, pH 4.0. The column was washed with three column volumes of 50 mM acetate, pH 4.0, then eluted with approximately three column volumes of 50 mM acetate, pH 5.5. All steps were performed at a linear flow rate of 300 cm/h. A final anion-exchange step on the Sartobind Q membrane (Sartorius) was applied to reduce endotoxin level of the Adnectin samples: Sartorius Sartobind Q anion-exchange membrane (7 ml) was conditioned with an excess volume of 50 mM acetate, 50 mM NaCl, pH 5.5. The cation-exchange eluate was diluted 1:2 with 20 mM histidine, pH 6.0, to a final pH of 5.5, adjusted to 50 mM NaCl (Glypican-3-binding Adnectins) or to 100 mM NaCl (A-RGE-H), then loaded onto Sartobind Q membrane, at up to 550 mg/ml, at a flow rate of 100 ml/min. The product was collected in the flow-through of the membrane.

The tubulysin analog used in this study, 'tub', was assembled by convergent synthesis from (2S,4R)-4-(2-((1R3R)-1-acetoxy-4-methyl-3-((2S,3S)-3-methyl-2-((R)-1-methylpiperidine-2-carboxamido)-N-propylpentanamido)pentyl)thiazole-4-carboxamido)-5-(4-aminophenyl)-2-methylpentanoic acid and a valine–citrulline linker with a maleimide functional group, using standard published processes (Patterson *et al.*, 2008) and was fully characterized (US Patent 8394922).

To conjugate compound 'tub' to an Adnectin with a C-terminal cysteine, a solution of purified Adnectin at approximately 10 mg/ml was dialyzed using tangential flow filtration (TFF) for 1 h, with the transmembrane pressure of 24 psi, into 50 mM sodium acetate, pH 5.3, 50 mM NaCl, and diluted to 6 mg/ml. The tubulysin analog (Fig. 1B) was dissolved in DMSO to 92 µM and added to the Adnectin at 10% excess. The mixture was filtered through a 0.22-µm PES sterile filter (Corning) and incubated at 21°C until all the proteins were conjugated, as evidenced by reverse-phase analytical HPLC monitored at 220 nm. Typically, this reaction was completed within 24 h. The sample was subjected to TFF to remove free tubulysin analog, to change the buffer to 50 mM NaCl, pH 5.3 and to concentrate the Adnectin–drug conjugate to approximately 10 mg/ml.

To prepare the tritium-labeled Adnectin–drug conjugates for quantitative whole body autoradiography (QWBA), 2 mg of A1H or A-RGE-H were incubated in 2 ml 50 mM NaOAc, pH 5.5, 10 mM NaCl, 5 mM TCEP, for 30 min at room temperature. TCEP was removed by filtration on a 5-ml HiTrap desalting column (GE) pre-equilibrated with 50 mM NaOAc, pH 5.5, 10 mM NaCl. To the desalted sample, 5.2 mCi (0.9 molar equivalents) of payload containing [^{3}H]-labeled tubulysin analog (Fig. 1B), in 7 mM DMSO, were added. The mixture was incubated for 4 h at room temperature. Five molar equivalents of unlabeled tubulysin analog, in 60 µl of 7 mM DMSO, were then added. The mixture was incubated first for 2 h at room temperature, then overnight at 7°C. After these incubations, the sample was diluted to 5 ml with 50 mM NaOAc, pH 5.5, 10 mM NaCl (Buffer A). The conjugate was purified by cation-exchange chromatography on a 1-ml HiTrap SP-HP column mounted on an AKTA Explorer (GE), using a 0–60% gradient of Buffer A and Buffer B (50 mM NaOAc, pH 5.5, 1 M NaCl) over 10 ml, at the flow rate of 1 ml/min. The fractions containing the conjugate were pooled and dialyzed against 20 mM histidine, pH 6.0, 10% sucrose, overnight, at 7°C. Radioactivity of the dialyzed conjugate was measured by liquid scintillation counting on TriCarb 2900 TR (PerkinElmer), and radiochemical purity of the conjugate was measured by analytical size-exclusion chromatography (SEC) using a Shodek KW403-4F, 4.6 × 300 mm, three-micron column, 100 mM sodium phosphate, pH 7.3, 150 mM NaCl running buffer, and flow rate of 0.3 ml/min. For A1H and A-RGE-H, specific activity was adjusted to 990 µCi/mg and 1.22 mCi/mg, respectively, by further addition of the unlabeled Adnectin–drug conjugate. Throughout the protocol, radioactivity was measured by liquid scintillation counting on a Perkin Elmer TriCarb 2900 TR, and protein concentration was measured on a Thermofisher Nandrop 2000c spectrophotometer.

The amount of endotoxin in samples was estimated using the Endosafe Multi Cartridge System (Charles River).

Molecular modeling and visualization

A homology model of A-RGE was built using MOE software (Chemical Computing Group ULC), with the Protein Data Bank (Berman *et al.*, 2000) crystal structure 1FNA (Leahy *et al.*, 1996) of the 10th human fibronectin type III domain as the template. A model of the tubulysin analog was built from the crystal structure GAFWAM (Steinmetz *et al.*, 2004) in the Cambridge Structural Database, using ConQuest software (Cambridge Crystallographic Data Centre, (Bruno *et al.*, 2002)). MOE was applied to modify the tubulysin template and combine it with the Adnectin homology model. The resulting model of the conjugate was relaxed by iterative conformation sampling and energy minimization in MOE and visualized in PyMOL (Schrodinger, LLC) and is shown in Fig. 1A.

Biophysical and biochemical properties

Molecular weight and chemical homogeneity of Adnectin–drug conjugate samples were confirmed by electrospray ionization

time-of-flight (ESI-TOF) mass spectroscopy, in line with reversed-phase chromatography. A 1290 LC system (Agilent) was coupled to a 6540 UHD Accuracte-Mass Q-TOF mass spectrometer (Agilent). Three micrograms of sample were injected onto an Agilent Zorbax C8 RRHD 2.1 mm × 50 mm column with 1.8 µm particle size. The mobile phases were 0.1% formic acid in water (mobile phase A) and 0.1% formic acid in acetonitrile (mobile phase B). The LC gradient profile was as follows (min/% of mobile phase B): 0/1, 1/2, 3/95, 3.5/95, 7/50, 8.5/1. Total run time was 9 min. The flow rate was 0.5 ml/min, and the column temperature was 40°C. The ESI-TOF was run in positive ion mode, with a capillary voltage of 4000 V, fragmentor of 175 V and *m/z* range of 500–3200. The deconvolution of electrospray ionization mass spectra was performed using MassHunter Qualitative Analysis software (Agilent).

Analytical SEC to evaluate the state of association of Adnectin–drug conjugates was performed at room temperature, using a 4.6 mm I.D × 300 mm length Shodex KW403-4F column (Showa Denko America) mounted on an Agilent 1260 HPLC with a binary pump. Ten micrograms of sample were injected onto the column. The running buffer was 100 mM sodium phosphate, 150 mM sodium chloride, pH 7.3, the flow rate was 0.3 ml/min and absorbance was monitored at 280 nM. The areas under each peak were integrated, and the area under the peak eluting between 17 and 1.3 kDa was used to estimate the fraction of monomeric Adnectin or Adnectin–drug conjugate in the sample. The estimates from two independent experiments were averaged to obtain the value shown in Table II.

Thermostability of Adnectin–drug conjugates was measured by differential scanning calorimetry (DSC) using a Microcal VP Capillary DSC (Malvern Instruments). The sample volume was 400 µl, the protein concentration was 0.5 mg/ml and the sample buffer was PBS. The scans, from 15°C to 110°C, were carried out at 60°C/h, with a filtering period of 16 s for data point collection. The data were analyzed using Origin 7 for Microcal VPDSC (Origin Lab).

Formation of iso-aspartate in Adnectin–drug conjugates A1-tub and A2-tub was quantified by incubating the Adnectin–drug conjugates at 5 mg/ml for 3 weeks at 40°C, in either 20 mM Tris, 200 mM NaCl, pH 7.0 or 20 mM histidine, 150 mM NaCl, pH 6.0. Next, the samples were denatured with 0.5% sodium dodecyl sulfate (SDS) in 50 mM ammonium bicarbonate, pH 7.2, at 37°C, for 1 h. After denaturation, SDS was diluted to 0.02% by the addition of more 50 mM ammonium bicarbonate, pH 7.2. The sample was digested with trypsin at protease:protein ratio of 1:10 (w/w), 37°C, for 6 h. The resulting peptides were analyzed by an Agilent 1200 HPLC coupled with a Thermo LTQ-XL mass spectrometer. Approximately 10 µg of each digested sample was separated on a Varian C8-A column (3 µm particle size, 2.0 × 150 mm) at 55°C, 0.2 ml/min. The mobile phase A was 0.1% TFA in water, and mobile phase B was 0.1% TFA in 90% ACN. UV absorbance of the eluent was monitored at 214 nm. The mass spectrometer was operated in positive ion mode with a full mass scan from 300 to 2000 *m/z*. The temperature of ion transfer tube of the linear ion trap was 270°C, and the electrospray voltage was 5.0 kV. The normalized collision energy in CID was 35%.

The peptide peaks representing the peptides containing aspartate or iso-aspartate on the FG loop (ITYGETGGNSPVQEFTVPGEHVTATISGLKPGVDYTITVYAVTYDGEK for A1-tub and ITYGETGGNSPVQEFTVPGEHVTATISGLKPGVDYTITVYAVTYDAEK for A2-tub) were identified based on their relative retention times and MS/MS data. The relative areas of the peaks were used to estimate the fraction of aspartate isomerized: % Isomerization = [MS Area isoAsp peptide/(MS Area native peptide + MS Area isoAsp)] × 100%.

Binding to human Glypican-3 was evaluated using a Biacore T100 surface plasmon resonance (SPR) instrument (GE Healthcare). Recombinant human or murine Glypican-3 proteins (R&D Systems) were diluted to 10 µg/ml in 10 mM sodium acetate, pH 4.5 and amine-coupled onto a CM5 biosensor (GE Healthcare). Adnectin and Adnectin–drug conjugate samples were diluted to concentrations between 200 and 1.56 nM in HBS-P+ running buffer (10 mM HEPES, 150 mM NaCl, 0.05% (*v/v*) Surfactant P20) and injected at 30 µl/min, 37°C. An injection of 10 mM glycine, pH 1.7, was used to regenerate the biosensor surfaces between assay cycles. Kinetic rate constants were derived from reference-subtracted sensorgrams fit to a 1:1 binding model in Biacore T200 Evaluation Software v2.0 (GE Healthcare), using the average of three independent experiments.

Specificity of the Glypican-3-binding Adnectin A1-alk was evaluated by diluting recombinant human Glypican-1, Glypican-2, Glypican-3, Glypican-5 and Glypican-6 proteins (R&D Systems) to 10 µg/ml in 10 mM sodium acetate, pH 4.5, then amine-coupling each Glypican onto one flow cell of a CM5 biosensor (GE Healthcare). Adnectin A1-alk was diluted to 1 µM, and α-Glypican antibody controls (R&D Systems) were diluted to 200 nM, in HBS-P+ running buffer (10 mM HEPES, 150 mM NaCl, 0.05% (*v/v*) Surfactant P20). Adnectin and antibody solutions were injected over the immobilized Glypican proteins at 10 µl/min, 25°C. An injection

Table II. *In vitro* properties of Glypican-3-binding and control Adnectins and Adnectin–drug conjugates

Adnectin ID	Mono (%)	T_m (°C)	Human Glypican-3			Murine Glypican-3			Hep3B-binding EC_{50} (nM)	Hep3B cytotox IC_{50} (nM)
			k_{on} (10^4 $M^{-1}s^{-1}$)	k_{off} (10^{-4} s^{-1})	K_d (nM)	k_{on} (10^4 $M^{-1}s^{-1}$)	k_{off} (10^{-4} s^{-1})	K_d (nM)		
A-RGE-alk	71	ND	No binding			No binding			ND	ND
A-RGE-tub	99	81°	No binding			No binding			No binding	314 ± 16
A-RGE-H-tub	96	ND	No binding			No binding			No binding	ND
A0	95	73°	20 ± 12	171 ± 18	110 ± 70	0.05 ± 0.02	8.0 ± 0.2	1600 ± 630	>1000	ND
A1-alk	98	93°	8.6 ± 0.2	6.8 ± 0.1	7.9 ± 0.4	7.1 ± 0.1	6.8 ± 0.2	9.6 ± 0.4	6.2 ± 0.2	ND
A1-tub	99	87°	12.0 ± 0.3	6.81 ± 0.04	5.7 ± 0.1	9.67 ± 0.05	6.67 ± 0.07	6.90 ± 0.04	2.8 ± 0.1	ND
A1H-tub	96	76, 84, 91°	8.9 ± 1.0	4 ± 2	5 ± 3	10 ± 3	4 ± 2	4 ± 2	ND	ND
A2-alk	98	86°	7.3 ± 0.9	21.3 ± 1.5	29.6 ± 2.5	7.6 ± 1.0	20.7 ± 1.6	27.8 ± 5.9	4.4 ± 0.2	>1000
A2-tub	99	79, 85°	6.7 ± 0.6	21.4 ± 1.5	32.2 ± 5.2	6.1 ± 0.5	20.3 ± 1.1	33.4 ± 4.3	2.6 ± 0.1	0.3 ± 0.1

Mono: fraction of sample present as soluble monomer, determined by SEC. T_m: melting temperature, determined by differential scanning calorimetry. k_{on}, k_{off}, K_d: kinetic binding constants determined by surface plasmon resonance (n = 3). EC_{50}: effective concentration with 50% binding. IC_{50}: effective concentration with 50% cytotoxicity. ND: not determined.

of 10 mM glycine pH 1.7 was used to regenerate the biosensor surfaces between assay cycles. Reference sensor-subtracted sensorgrams were aligned in Biacore T100 Evaluation Software (GE Healthcare) and plotted using GraphPad Prism v7.

In vitro *cell binding and cytotoxicity*

Binding of Adnectins and Adnectin–drug conjugates to Hep3B cells (ATCC #HB-8064) was quantified by flow cytometry. The cells were seeded at 200 000 cells per well in Stain Buffer (BD Pharmingen) and incubated with triplicate independent serial dilutions of Adnectins, for 1 h, at 4°C, in 100 µl. Following three washes with Stain Buffer, the bound Adnectins were detected using mouse monoclonal antibody 1513.2300.16F7.E7.E1 (BMS; 7 µg/ml in Stain Buffer), specific for an epitope outside the diversified loops, and a PE-conjugated, anti-mouse, secondary antibody (Jackson; 2.5 µg/ml in Stain Buffer). The cells were analyzed using a BD FACSCantoII instrument, using detection at 575 nm. Mean fluorescent intensities (MFIs) of the cell populations were calculated using FlowJo v10, and EC_{50} values were fit to a four-parameter algorithm using GraphPad Prism v7.

Cytotoxicity of Adnectin–drug conjugates was observed by monitoring ATP production in viable carcinoma cells, using a CellTiter-Glo assay (Promega). Glypican-3-positive Hep3B cells were seeded in 96-well plates at 2000 cells per well. Adnectin–drug conjugates were serially diluted from 1 µM and added to the Hep3B wells in triplicate, to the total volume of 100 µl. Hep3B plates were incubated for 6 days at 37°C. Glypican-3-negative JAR cells were seeded in 96-well plates at 10 000 cells per well. Adnectin–drug conjugates were serially diluted from 100 nM and added to the JAR wells in duplicate, to the total volume of 100 µl. JAR plates were incubated for 4 days at 37°C. After the incubation, cells were lysed using 100 µl CellTiter-Glo assay reagent (Promega), following manufacturer protocol. Luminescence was quantified on an EnVision plate reader (PerkinElmer), and data were normalized against untreated control wells. IC_{50} values were fit to a five-parameter, non-linear, curve-fit algorithm using GraphPad Prism v7.

Biodistribution

Female NSG mice (NOD.Cg-Prkdcscid Il2rgtm1Wjl/SzJ) with Hep3B tumors of 100–220 mm^3 on their left flank were administered a single IV dose of [^{3}H]-labeled A-RGE-H-tub or A1H-tub, each at 0.22 µmol/kg. After 24 and 168 h, one mouse per Adnectin–drug conjugate was euthanized. Each carcass was frozen immediately by immersion in a liquid nitrogen bath for 2–4 min, then stored at −20°C until embedding.

Frozen mouse carcasses were prepared for quantitative whole body autoradiography following established methodology (Ullberg, 1954). The carcasses were embedded with a microtome stage in an ice-cold solution of 2% carboxymethylcellulose, then frozen in a dry ice-hexane bath at −70°C for approximately 60 min, followed by overnight storage at −20°C. Whole body sections in the sagittal plane, 40 µm thick, were obtained in a Leica CM3600 crymicrotome (Leica microsystems). The sections were captured on adhesive tape (Scotch Tape No. 8210, 3 M Ltd) at −20°C and dried in the cryomicrotome, at −20°C, for 5 days. The sections of each animal were mounted on cardboard and exposed, along with calibration ^{3}H standards (Amersham Life Sciences), to a ^{3}H-sensitive phosphor imaging plate (GE Healthcare Life Sciences), for 46 days at room temperature. After exposure, the imaging plates were scanned using Typhoon FLA-7000 image acquisition system (GE Healthcare Life Sciences). The resulting whole body images were stored on a dedicated computer server. Quantification was performed by image densitometry using MCID image analysis software 7.0 (Imaging Research, Inc.). Concentrations of the radioactive tubulysin analog (Fig. 1B) in tissues were interpolated from each standard curve as nanocuries per milligram tissue (nCi/mg tissue). Radioactivity in the calibration standards ranged from 0 to approximately 10 nCi/mg tissue, and the R^2 values obtained for the calibration curves ranged from 0.9994 to 0.9999, which demonstrated the linearity of imaging plate response. The lower limit of quantification was determined as the mean concentration value of radioactivity of the background in the imaging plates without tissues (mean of 10 measurements per imaging plate, using sampling tools provided by the MCID image analysis software).

To determine the fraction of injected dose localized to the tumor, the length and width of each tumor were measured in whole body images using MCID image analysis software. The volume of a tumor was calculated with ellipsoid volume formula (Jensen *et al.*, 2008).

$V = 1/2\ (L \times W^2)$, where L is length and W is with width of the tumor.

The tumor weight was calculated from the volume and density (1.05 g/ml) (Jensen, Jorgensen, Binderup and Kjaer, 2008). The percent of injected dose in a tumor was calculated based on the measured radioactivity in the tumor (in nCi/mg tissue), the tumor weight and the radioactivity dose administered to the mouse.

Pharmacokinetics in mice

The systemic exposure profile of the Glypican-3-binding Adnectin–drug conjugate, A2-tub, was determined in female NOD/SCID mice bearing Hep3B xenograft tumors with an average volume of 220 mm^3. Four mice per time point were dosed intravenously, each with a single dose of 0.5 µmol/kg A2-tub. At time points of 0.3, 1, 2, 4, 8, 24, 48, 72 and 96 h, blood samples were collected, serially, from the tail vein, using CPD anticoagulant (citrate–phosphate–dextrose solution, Sigma). Plasma obtained from these blood samples were aliquoted and stored at −80°C until analysis. Plasma levels of A2-tub were determined using a standard Gyrolab ligand-binding assay (Roman *et al.*, 2011), where A2-tub was captured by antibodies against the regions of Adnectins conserved between ^{10}Fn3 and Adnectins (1513.2300.16F7.E7.E1, BMS) and detected by antibodies against tubulysin (1200.1696.8F3.H3, BMS). Pharmacokinetic parameters were calculated using non-compartmental, Phoenix WinNonlin analysis.

Efficacy in mouse xenograft models

Female NOD/SCID mice, 7–8 weeks of age, with an average weight of approximately 22 g, were inoculated subcutaneously in the right flank with 5×10^6 Hep3B cells. Approximately 2 weeks after implantation, when the tumors reached an average tumor volume of 250 mm^3, tumor-bearing mice were randomized into treatment groups (n = 8–10 per treatment). Adnectin–drug conjugate A-RGE-tub or A2-tub in 50 mM NaOAc, 150 mM NaCl, pH 5.5, were administered by intravenous injection. The schedules described in this study are once a week for 3 weeks, every other week for 6 weeks, and single dose. The animals were monitored twice weekly for body weight and tumor size. Tumor volume was estimated using the formula $TV = a \times b^2/2$, where 'a' and 'b' are the long and the short diameter of a tumor, respectively. Animal care, handling and treatment procedures were performed according to guidelines approved by the Institutional Animal Care and Use Committee of

BMS and following the guidance of the Association for Assessment and Accreditation of Laboratory of Animal Care.

Results

Discovery of Glypican-3-binding Adnectins

Adnectins that bind Glypican-3 were discovered by applying a combination of mRNA display and yeast surface display (Koide, Koide and Lipovšek, 2012) to a library based on the human 10th fibronectin type III domain (^{10}Fn3), where loops BC, DE and FG (structurally analogous of antibody complementarity determining regions) were randomized (Lipovšek, 2010). Naïve selection for binding to human Glypican-3 from a library of 5×10^{13} unique sequences yielded Adnectin A0, which bound human Glypican-3 with the K_d of approximately 110 nM but showed at least 10-fold weaker binding to murine Glypican-3 (Tables I and II, Supplementary Table SI).

A0 was affinity-matured under selection conditions that were highly stringent for binding to human Glypican-3, with an emphasis on slow dissociation rate. The resulting Adnectin with the best combination of affinity for human and murine Glypican-3, solubility and thermostability was further engineered. First, we introduced a single cysteine at the C-terminus to generate Adnectin A1, which bound human and murine Glypican-3 with the K_d of 7.9 and 9.6 nM, respectively (Tables I and II), and that, at 100 nM Adnectin, showed no binding to immobilized human Glypican-1, Glypican-2, Glypican-5 or Glypican-6 (Supplementary Fig. S3). Second, we mutated the dipeptide Asp-Gly, found in loop FG, which is prone to aspartate isomerization, into the isomerization-resistant dipeptide Asp-Ala, to generate Adnectin A2, which bound human and murine Glypican-3 with the K_d of 30 and 28 nM, respectively (Tables I and II). Throughout this study, properties of Adnectins A0, A1 and A2 were compared to the non-binding, control Adnectin, A-RGE. A-RGE differs from wild-type human ^{10}Fn3 only in the mutation of the integrin-binding tripeptide Arg-Gly-Asp on the wild-type FG loop into the non-binding Arg-Gly-Glu (Table I); as a consequence, A-RGE can serve as an inert, non-binding control for both *in vitro* and *in vivo* studies.

Preparation of Adnectin–tubulysin conjugates

The Adnectins described in this study were expressed in *E. coli* and purified from the soluble cytoplasmic fraction. The yields of Adnectin A-RGE and of the Glypican-3-binding Adnectins A1 and A2, after fermentation and purification, were approximately 0.4 g/l. The monomeric Glypican-3-binding Adnectins constituted 97–99% of the purified sample, as judged by analytical SEC (Table II). Conjugation of purified Adnectins through C-terminal cysteine to a maleimide-containing payload comprising a linker and a tubulysin analog (Fig. 1B) was accomplished with 96% conversion, as demonstrated by analytical HPLC. The radiochemical purity of monomeric, conjugated, tritium-labeled Adnectin–drug conjugates, as measured by analytical SEC, was 99% for A1-H-tub and 100% for A-RGE-H-tub. The high conversion rate and the high specificity translate into the Adnectin–drug ratio of 1.0 for all the conjugates described in this study. All Adnectin–drug conjugate samples used in cytotoxicity or in *vivo* studies had endotoxin levels lower or equal to 0.1 EU per milligram of protein.

Biophysical and biochemical properties

State of association, stability and target-binding properties of Adnectins A-RGE, A0, A1 and A2 are summarized in Table II and illustrated by Supplementary Figs S2 and S3. For the Adnectins formatted with a C-terminal cysteine, both the version where the C-terminal cysteine was alkylated (e.g. A1-alk) and where the C-terminal cysteine was conjugated to cytotoxic payload (e.g. A1-tub) were characterized.

The affinity-matured Glypican-3-binding Adnectins, A1-alk and A2-alk, as well as their conjugates that contain the tubulysin analog, A1-tub and A2-tub, were highly monomeric (≥98%) and thermostable ($T_m \geq 85$°C) at neutral pH, in a simple phosphate buffer.

The cytotoxic payload conjugate of the original affinity-matured Adnectin, A1-tub, which contains the Asp-Gly dipeptide in its FG loop, was susceptible to aspartate isomerization (Wakankar and Borchardt, 2006), showing 9% conversion from aspartate to isoaspartate after a 3-week 40°C incubation at pH 7.0, and 12% conversion after a 3-week 40°C incubation at pH 6.0. Adnectin A2-tub, which contains the mutation from Asp-Gly to Asp-Ala, showed a lower level of isomerization, with 2.4% conversion after 3-week 40°C incubation at pH 7.0, and 3.6% conversion at pH 6.0 (data not shown).

Adnectin A1 showed a K_d of approximately 8 (±2) nM for human and murine Glypican-3, regardless of its state of conjugation. Adnectin A2 showed a reduced affinity for human and murine Glypican-3, with a surface plasmon resonance K_d of approximately 31 (±3) nM, again regardless of whether its C-terminal cysteine had been alkylated or conjugated to a tubulysin analog-containing payload.

In vitro cell binding and cytotoxicity

Despite its approximately 4-fold lower affinity for Glypican-3 as measured by surface plasmon resonance, A2, the affinity-matured Adnectin resistant to aspartate isomerization, bound to the Hep3B cell line, which overexpresses human Glypican-3, with the same EC_{50} as A1, the original affinity-matured Adnectin, under the assay conditions. Regardless of C-terminal alkylation or conjugation to a tubulysin analog-containing payload, the cell-binding EC_{50} of A1 and A2 was approximately 4 (±2) nM. In contrast, the non-binding control Adnectins, A-RGE-alk and A-RGE-tub, showed no detectable binding to Hep3b (Table II, Fig. 2A).

The Adnectin—drug conjugate form of A2, A2-tub, was highly toxic to Glypican-3-positive Hep3B cells, with the IC_{50} of 0.3 nM. In contrast, the non-binding Adnectin–drug conjugate control, A-RGE-tub, showed cytotoxicity lower by three orders of magnitude, with the estimated IC_{50} of 310 nM (Table II, Fig. 2B). As expected, A2-alk, the Glypican-3-binding Adnectin without the tubulysin analog-containing payload, was not toxic to cells.

A test on Glypican-3-negative JAR cells (Khan *et al.*, 2001) showed minimal cytotoxicity of Adnectin–drug conjugates at 10 nM, and no difference in cytotoxicity between a Glypican-3-binding Adnectin–drug conjugate, A1-tub, and the non-binding control Adnectin, A-RGE-tub (Supplementary Fig. S4).

Biodistribution

Quantitative whole body autoradiography of mice with Hep3B xenografts that had been dosed with tritium-labeled Adnectin–drug conjugates (Fig. 3) shows that the Glypican-3-binding Adnectin–drug conjugate, A1H-tub, but not the conjugate with non-binding Adnectin, A-RGE-H-tub, localized specifically to tumors that overexpress Glypican-3. For both Adnectin–drug conjugates, exposure of normal tissues was minimal, with the exception of the kidney, which is the expected organ of elimination.

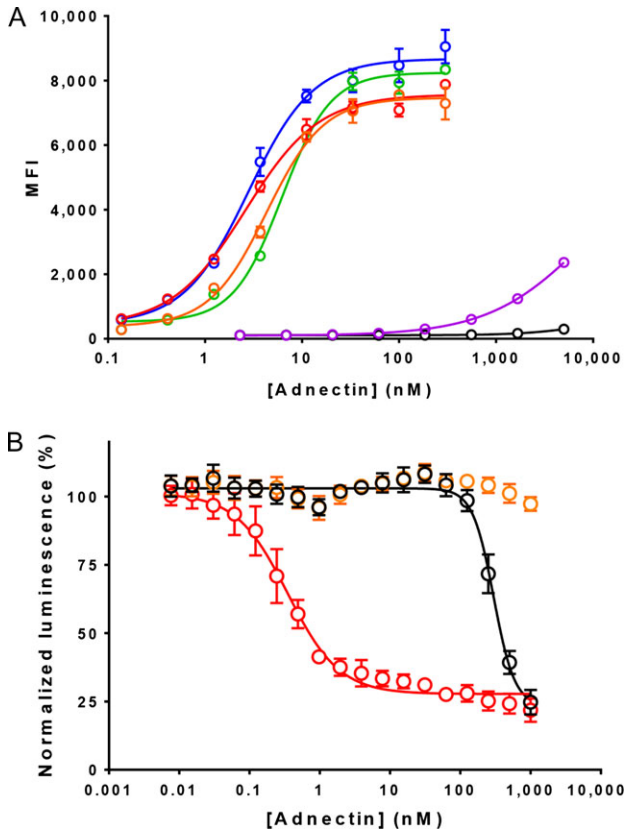

Fig. 2 Properties of Glypican-3-binding Adnectins and Adnectins conjugated to tubulysin analog on cultured Hep3B cells. [Adnectin]: concentration of alkylated or tubulysin-conjugated Adnectin. A-alk: Adnectin with alkylated C-terminal cysteine. A-tub: Adnectin conjugated to tubulysin analog. Error bars represent standard deviations from the mean for three independent experiments. (**A**) Cell binding, as detected by analytical flow cytometry. MFI: mean fluorescence intensity at 575 nm as a measure of the number of Adnectin molecules bound per Hep3B cell. Purple: A0; blue: A1-tub; green: A1-alk; red: A2-tub; orange: A2-alk; black: A-RGE-tub. (**B**) Cytotoxicity, as detected by loss of ATP production of Glypican-3-positive HepB cells. Normalized luminescence: ratio of luminescence of Hep3B samples incubated with Adnectin or Adnectin–drug conjugate vs. Adnectin-free Hep3B. Red: A2-tub; orange: A2-alk; black: A-RGE-tub.

Five hours after the administration of A1H conjugated to tritium-labeled tubulysin (A1H-tub), the radioactive signal was high in the tumor and in the kidney (Fig. 3A and C). The detectable signal in two other normal tissues (liver and lung) was lower by more than an order of magnitude, and the signal in blood, blood marrow, brain and skeletal muscle was undetectable. At the same, 5-h time point, the radioactive signal from the non-binding control Adnectin–drug conjugate, A-RGE-H-tub, was found primarily in the kidney (Fig. 3B and C).

A week after administration, a strong signal remained in the tumors of animals treated with A1H-tub, but not in their normal tissues, and not in animals treated with the non-binding A-RGE-H-tub (Fig. 3D).

The fraction of injected dose of Adnectin–drug conjugate in the Glypican-3-positive tumor, 5 h after administration, was estimated to be 1.0% for A1H-tub and 0.09% for A-RGE-H-tub. One week after administration, the fraction of injected dose in the tumor was approximately 1.3% for A1H-tub and 0.06% for A-RGE-H-tub.

Pharmacokinetics in mice

A2-tub, the Glypican-3-binding Adnectin A2 conjugated to a tubulysin analog, was administered to NOD/SCID mice carrying approximately 220 mm^3 xenograft tumors derived from Hep3B. A single dose of 0.5 μmol/kg was eliminated from plasma with the half-life of approximately 0.5 h (Table III).

Efficacy in mouse xenograft models

Glypican-3-binding Adnectin A2 conjugated to tubulysin, A2-tub, and the non-binding control Adnectin–drug conjugate, A-RGE-tub, were administered to mice carrying approximately 220 mm^3 Hep3B xenograft tumors. Weekly administration of A2-tub inhibited growth and caused regression of Hep3B tumor xenografts in a dose-dependent manner. Three weekly, 0.12 μmol/kg, doses of A2-tub eliminated the tumors completely; no tumors regrew during the 3-week observation after the treatment had been completed. In contrast, weekly administration of A-RGE-tub at 0.12 μmol/kg allowed the tumors to continue growing (Fig. 4A).

Even when administered every other week or in a single dose, at 0.04 μmol/kg, A2-tub suppressed tumor growth for approximately 5 and 3 weeks, respectively; an equivalent single dose of A-RGE-tub allowed the tumors to grow (Fig. 4C).

The mice that received weekly doses of A2-tub and A-RGE-tub at up to 0.12 μmol/kg stayed within 10% of their starting body weight (Fig. 4B), maintained a body condition score of 3 (Ullman-Culleré and Charmaine, 1999), and showed no abnormal clinical signs during the study period. In particular, the mice did not present any signs of pain or distress or any palpable or observable anomalies and retained normal hydration, alertness, activity and gregarious behavior.

Discussion

To examine the suitability of Adnectin–drug conjugates for targeted cancer therapy, we conjugated two Glypican-3-binding Adnectins to a payload that comprised a protease-cleavable linker and a cytotoxic tubulysin analog. We tested the resulting model conjugates for their ability to bind to human and murine Glypican-3 *in vitro*; to distribute specifically to Glypican-3-positive tumors and clear from normal tissues *in vivo*; and to kill cells that overexpress Glypican-3 both *in vitro* and *in vivo*.

Whereas the ability to select Adnectins with high affinity and specificity using library-based protein engineering (Lipovšek, 2010) and fast clearance of proteins smaller than 60 kDa from humans and model organisms (Lin, 2009) had been well established before the outset of this study, a major open question was whether a targeting protein with a half-life of less than an hour could provide sufficient exposure to the tumor that overexpresses its target to inhibit its growth. Will enough Glypican-3-binding Adnectin–drug conjugate bind to the Glypican-3-positive tumor to provide a signal above the background of normal tissues? Will the monovalent binding of the Adnectin to Glypican-3 enable internalization of the Adnectin–tubulysin conjugate, and thus targeted cytotoxicity?

The two Adnectins that were used to answer this question, A1H and A2, differ in a single FG loop mutation, which removes an aspartaten isomerization-prone dipeptide from A1H, and in the presence of hexahistidine tag in A1H (Table I). Despite an approximately 4-fold lower affinity of A2 for Glypican-3 in a kinetic assay, their binding to Glypican-3 displayed on cultured Hep3B cells is indistinguishable (Table II).

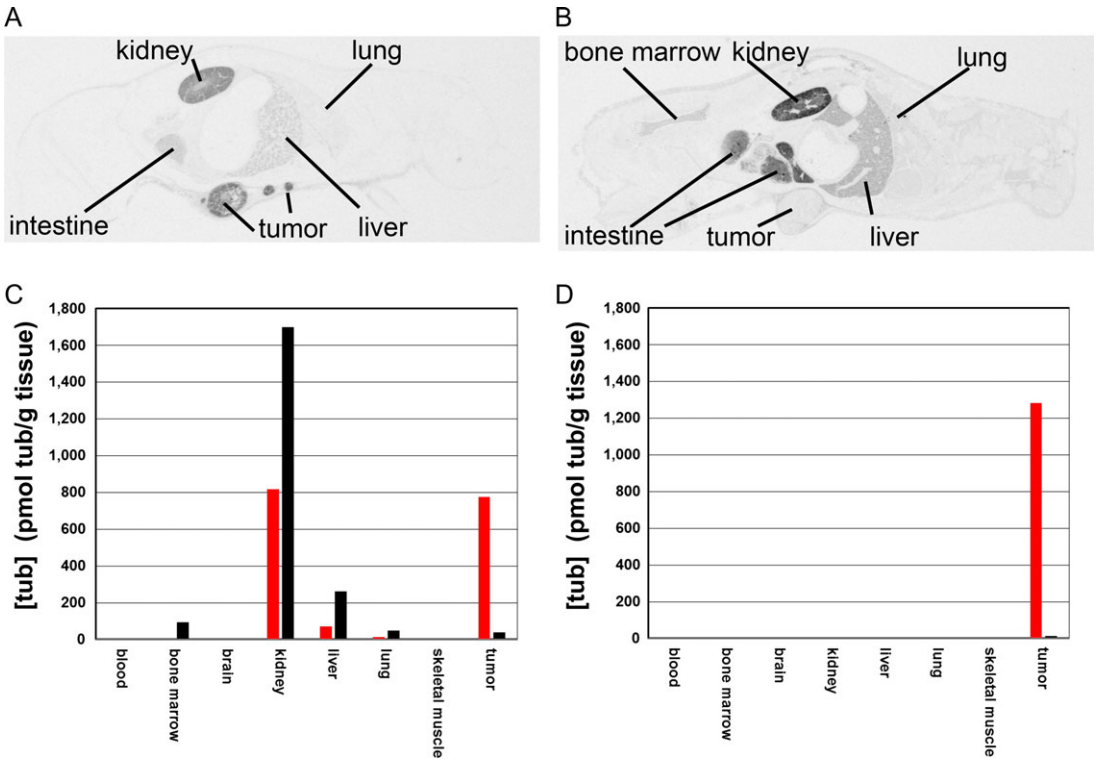

Fig. 3 Biodistribution of Adnectins conjugated to [3H]-tubulysin analog in mice harboring Glypican-3-positive tumors derived from Hep3B cells. Whole body autoradiograph of a mouse sacrificed 5 h after administration of [3H]—A1H-tub (**A**) and [3H]—A-RGE-H-tub (**B**). Quantified radioactivity in selected tissues, 5 h (**C**) and 168 h (**D**) after the administration of [3H]—A1-H-tub (red bars) vs. [3H]—A-RGE-H-tub (black bars).

Table III. Pharmacokinetic parameters for Glypican-3-binding Adnectin A2 conjugated to tubulysin, A2-tub, administered intravenously, at 0.5 μmol/kg, to NOD/SCID mice carrying approximately 220 mm^3 Hep3B-derived xenograft tumors

AUC (INF) (μg h/ml)	$T_{1/2}$ (h)	MRT (h)	CLT (ml/ h kg)	Vss (L/kg)
435	0.53	0.59	1.2	0.67

AUC (INF): area under the curve. $T_{1/2}$: elimination half-life. MRT: mean residence time; CLT: total clearance; Vss: steady-state volume of distribution.

Our results show that optimized Glypican-3-binding Adnectin–drug conjugate, A2-tub, does kill Hep3B cells, which overexpress Glypican-3, both in suspension of cultured cells (Fig. 2B) and in xenograft tumors on mice (Fig. 4A and B). The lack of cytotoxicity of A-RGE-tub, the conjugate between a non-binding control Adnectin and the same tubulysin analog, suggests that cytotoxicity is dependent on the binding between Adnectin A2 and its target, Glypican-3. This conclusion is further supported by the low cytotoxicity, indistinguishable from the cytotoxicity of the A-RGE-tub-negative control, of A1-tub on Glypican-3-negative JAR cells (Supplementary Fig. S4).

Quantitative whole body radiography of mice with Hep3B xenografts that were dosed with radiolabeled Adnectin–drug conjugates (Fig. 3) shows that the Glypican-3-binding Adnectin–drug conjugate, A1H-tub, but not the conjugate with non-binding Adnectin, A-RGE-H-tub, localizes specifically to tumors that overexpress Glypican-3. Strong radioactive signal that corresponds to approximately 1.3% of the injected dose remains in the Glypican-3-positive tumors of A1H-tub-treated mice even 7 days after administration (Fig. 3D); this is remarkable for a molecule with the half-life in the bloodstream of only half an hour. The week-long persistence in the tumor of radiolabeled payload delivered by Glypican-3-binding Adnectin–drug conjugate is consistent with their internalization into cells immediately upon binding, and with the payload (either as a part of intact Adnectin–drug conjugate or as the small-molecule tubulysin analog released by cleavage of the linker) remaining inside the cells, protected from renal filtration of the plasma. The undetectable signal in normal tissues 7 days after administration (Fig. 3D) demonstrates that on-target, off-tumor effects are extremely low for this molecule. This is significant because A1H binds as tightly to murine Glypican-3 as to human Glypican-3 (Table II) and thus would be expected to localize to any normal mouse tissue that expresses Glypican-3.

The high contrast between signal originating from radioactive Adnectin–drug conjugate in Glypican-3-positive xenograft tumors vs. in normal tissues differs dramatically from typical whole body autoradiographs of antibody–drug conjugates, which show strong signal in all perfused normal tissues. For example, a week-long QWBA study of an antibody–drug conjugate that binds to P-cadherin found the tumor-to-blood ratio of only 0.5 (maximal signal observed) or 1.5 (area under the curve) (Walles *et al.*, 2016).

The observed tumor uptake of the A1H-tub Glypican-3-binding Adnectin–drug conjugate and its persistence in the tumor 1 week after dosing appear to conflict with the modeled prediction that target-binding molecules in the 10 kDa range require sub-nanomolar affinity for the majority of injected drug to be localized to a human tumor (Schmidt and Wittrup, 2009). This discrepancy may be due to the efficient internalization of Glypican-3, which minimizes the loss of Adnectin–drug conjugate once it has bound its target. More

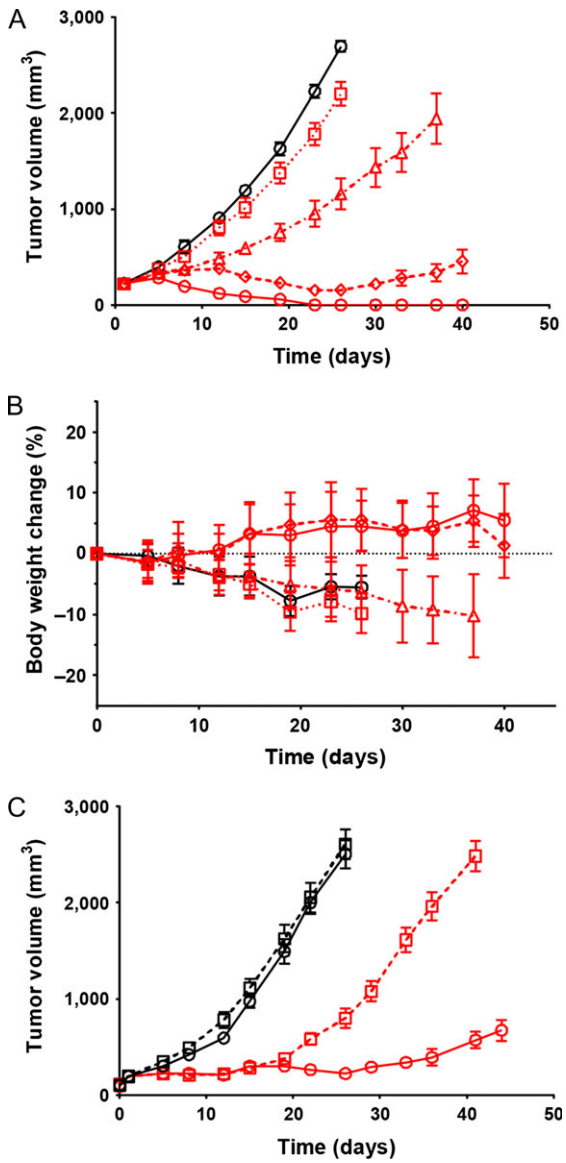

Fig. 4 Efficacy of Adnectin–drug conjugates against Hep3B xenograft tumors in nude mice, and variation of mouse body weight. Error bars represent standard deviation. (**A**) Dose dependence of efficacy with weekly administration. Black: Non-binding control, A-RGE-tub. Red: Glypican-3-binding Adnectin–drug conjugate, A2-tub. Circles, solid lines: 0.12 μmol/kg. Diamonds, dashed line: 0.04 μmol/kg. Triangles, dash/dotted line: 0.01 μmol/kg. Squares, dotted line: 0.004 μmol/kg. (**B**) Dose dependence of body weight with weekly administration. Black: Non-binding control, A-RGE-tub. Red: Glypican-3-binding Adnectin–drug conjugate, A2-tub. Circles, solid lines: 0.12 μmol/kg. Diamonds, dashed line: 0.04 μmol/kg. Triangles, dash/dotted line: 0.01 μmol/kg. Squares, dotted line: 0.004 μmol/kg. (**C**) Dependence of efficacy on schedule of administration, at 0.04 μmol/kg. Black: Non-binding control, A-RGE-tub. Red: Glypican-3-binding Adnectin–drug conjugate, A2-tub. Squares, dotted lines: single dose. Circles, solid lines: dosing every 14 days.

importantly, our goal has been not to maximize tumor uptake, but to deliver a sufficient dose to the tumor to cause regression (Fig. 4), while at the same time minimizing exposure of normal tissues (Fig. 3), and thus minimizing off-target toxicity. As long as these two requirements are met, the exact fraction of injected dose that is delivered to the tumor is not critical. In the mouse model described here, weekly delivery of only in the order of 1% of the injected dose to the tumor is sufficient for sustained tumor regression.

It is remarkable that, despite the Adnectin half-life in mice of less than half an hour, weekly administration of A2-tub at 0.12 μmol/kg is sufficient for complete and sustained regression of Hep3B xenografts, and that a single dose of A2-tub inhibits tumor growth for 2 weeks. Clearly, in the short time before being eliminated by renal filtration, sufficient A2-tub has bound and been internalized by the Glypican-3-overexpressing tumor cells for the tubulysin analog to kill cells and perhaps to trigger additional physiological processes such as cell-mediated cytotoxicity.

Whereas the low exposure of most normal tissues seen in quantitative whole body radiography (Fig. 3) and the stable body weight of mice treated in the efficacy study (Fig. 4B) are suggestive of low toxicity of Adnectin–drug conjugates, specialized toxicology studies in several species will be required to evaluate the toxicity and determine the therapeutic index of A2-tub. Adnectin–drug conjugates directed against additional targets will be necessary to evaluate how broadly this format can be applied. However, the excellent performance of ^{10}Fn3-derived positron emission tomography (PET) imaging agents, shown both for a ^{64}Cu-labeled imaging agent that binds EGFR (Hackel *et al.*, 2012) and for an ^{18}F-labeled Adnectin that binds human PD-L1 and that has pharmacokinetic properties indistinguishable from A1H and A2 (Donnelly *et al.*, 2017), suggests that crisp, target-dependent biodistribution is a property of the Adnectin family of therapeutic proteins, not unique to Glypican-3-binding Adnectins.

Conclusions

We show that an Adnectin–drug conjugate, a molecule of only 12 kDa and with a half-life in rodents of under an hour, can localize to a xenograft tumor that overexpresses the target of the Adnectin and can cause tumor inhibition and regression. The observations that weekly dosing of this short-lived molecule is sufficient for a sustained curative effect, and that a single dose of Adnectin–drug conjugate can inhibit tumor growth for 2 weeks, demonstrate that a long half-life in plasma is not required for efficacy in cancer models. As expected, the short half-life of Adnectin–drug conjugates limits exposure of normal tissues to the cytotoxic payload, suggesting that cytotoxic drug conjugates with small targeting domains such as Adnectins may have lower toxicity and higher therapeutic index than traditional antibody–drug conjugates. A rigorous test of this hypothesis will require a comparison of clinical efficacy and safety between antibody- and Adnectin-based therapeutics against Glypican-3, and against several other targets. We expect that other low-molecular weight target-binding scaffolds and biophysically robust antibody fragments may share a similarly beneficial balance of efficacy over toxicity.

Supplementary data

Supplementary data are available at *Protein Engineering, Design and Selection* online.

Acknowledgements

The authors thank Hendrik Adams and Pim Hermans of Bioaffinity Company for their assistance with setting up the BAC yeast surface display system; Herinder Lonial and Rolf Ryseck for cloning of human Glypican-3; Ginger Rakestraw, Paige Dickson and Jacqueline Olender for their

contributions to *in vitro* selections of Glypican-3-binding Adnectins; Heather Malakian, Brendan Nichols, Irina Zhan, Radhika Nayak and Bree Goldstein for molecular biology support; Mike Dabritz, Brendan Nichols, Joseph Toth, Li Ma and Weiqi Chen for protein chemistry support; Aaron Yamniuk, Yihong Zhang, Pallavi Gambhire, Lisa Megson, Huiming Li, Jen Morse and Simon Low for protein analytics; Fabienne Denhez, Katie Russo and Sarah Maas for *in vitro* binding assays; Amy Wiebesiek, Christopher Mulligan and Marc Fancher for *in vivo* support of QWBA; Tracy Mitchel and Kristen Fong for pharmacokinetic analysis; BMS Chemical and Synthetic Development and Akin Davulcu for the supply of the cytotoxic payload; Stanley Krystek for the molecular model of an Adnectin–drug conjugate, and for Fig. 1A; and Sharon Cload, Greg Vite, Ramaswamy Iyer and Mike Gosselin for support and strategic guidance.

Funding

This work was supported by Bristol-Myers Squibb Company.

Conflict of interest

All authors are current or former employees of Bristol-Myers Squibb Company, which funded the research described in this article.

References

Appelbaum,F.R. and Bernstein,I.D. (2017) Gemtuzumab ozogamicin for acute myeloid leukemia. *Blood*. doi:10.1182/blood-2017-09-797712.

Benatuil,L., Perez,J.M., Belk,J. and Hsieh,C.M. (2010) *Protein Eng. Des. Sel.*, **23**, 155–159. doi:10.1093/protein/gzq002.

Berman,H.M., Westbrook,J., Feng,Z., Gilliland,G., Bhat,T.N., Weissig,H., Shindyalov,I.N. and Bourne,P.E. (2000) *Nucleic Acids Res.*, **28**, 235–242.

Bross,P.F., Beitz,J., Chen,G. *et al.* (2001) *Clin. Cancer Res.*, **7**, 1490–1496.

Bruno,I.J., Cole,J.C., Edgington,P.R., Kessler,M., Macrae,C.F., McCabe,P., Pearson,J. and Taylor,R. (2002) *Acta Crystallogr. B*, **58**, 389–397.

Cox,N., Kintzing,J.R., Smith,M., Grant,G.A. and Cochran,J.R. (2016) *Angew. Chem. Int. Ed Engl.*, **55**, 9894–9897. doi:10.1002/anie.201603488.

Currier,N.V., Ackerman,S.E., Kintzing,J.R., Chen,R., Filsinger Interrante,M., Steiner,A., Sato,A.K. and Cochran,J.R. (2016) *Mol. Cancer Ther.*, **15**, 1291–1300. doi:10.1158/1535-7163.MCT-15-0881.

Dickinson,C.D., Veerapandian,B., Dai,X.-P., Hamlin,R.C., Xuong,N.-h., Ruoslahti,E. and Ely,K.R. (1994) *J. Mol. Biol.*, **236**, 1079–1092.

Donaghy,H. (2016) *MAbs*, **8**, 659–671. doi:10.1080/19420862.2016.1156829.

Donnelly,D.J., Smith,R.A., Morin,P. *et al.* (2017) *J. Nucl. Med.* doi:10.2967/jnumed.117.199596.

Dubowchik,G.M., Firestone,R.A., Padilla,L., Willner,D., Hofstead,S.J., Mosure,K., Knipe,J.O., Lasch,S.J. and Trail,P.A. (2002) *Bioconjug. Chem.*, **13**, 855–869.

Durocher,Y., Perret,S. and Kamen,A. (2002) *Nucleic Acids Res.*, **30**, E9.

Filmus,J. and Capurro,M. (2013) *FEBS J.*, **280**, 2471–2476. doi: 10.1111/febs.12126.

Fleming,B.D. and Ho,M. (2016) *Toxins (Basel)*, **8**. doi:10.3390/toxins8100274.

Goldberg,S.D., Cardoso,R.M., Lin,T., Spinka-Doms,T., Klein,D., Jacobs,S.A., Dudkin,V., Gilliland,G. and O'Neil,K.T. (2016) *Protein Eng. Des. Sel.*, **29**, 563–572. doi:10.1093/protein/gzw054.

Hackel,B.J., Kimura,R.H. and Gambhir,S.S. (2012) *Radiology*, **263**, 179–188. doi:10.1148/radiol.12111504.

Haruyama,Y. and Kataoka,H. (2016) *World J. Gastroenterol.*, **22**, 275–283. doi:10.3748/wjg.v22.i1.275.

Ikeda,M., Ohkawa,S., Okusaka,T., Mitsunaga,S., Kobayashi,S., Morizane,C., Suzuki,I., Yamamoto,S. and Furuse,J. (2014) *Cancer Sci.*, **105**, 455–462. doi:10.1111/cas.12368.

Ishiguro,T., Sano,Y., Komatsu,S.I. *et al.* (2017) *Sci. Transl. Med.*, **9**. doi:10.1126/scitranslmed.aal4291.

Jensen,M.M., Jorgensen,J.T., Binderup,T. and Kjaer,A. (2008) *BMC Med. Imaging*, **8**, 16. doi:10.1186/1471-2342-8-16.

Joubert,N., Denevault-Sabourin,C., Bryden,F. and Viaud-Massuard,M.C. (2017) *Eur. J. Med. Chem.* doi:10.1016/j.ejmech.2017.08.049.

Khan,S., Blackburn,M., Mao,D.L., Huber,R., Schlessinger,D. and Fant,M. (2001) *Histol. Histopathol.*, **16**, 71–78.

Koide,A., Bailey,C.W., Huang,X. and Koide,S. (1998) *J. Mol. Biol.*, **284**, 1141–1151. doi:10.1006/jmbi.1998.2238.

Koide,S., Koide,A. and Lipovšek,D. (2012) *Methods Enzymol.*, **503**, 135–156. doi:10.1016/b978-0-12-396962-0.00006-9.

Kurz,M., Gu,K. and Lohse,P.A. (2000) *Nucleic Acids Res.*, **28**, E83.

Lamb,Y.N. (2017) *Drugs*. doi:10.1007/s40265-017-0802-5.

Leahy,D.J., Aukhil,I. and Erickson,H.P. (1996) *Cell*, **84**, 155–164.

Lin,J.H. (2009) *Curr. Drug Metab.*, **10**, 661–691.

Lipovšek,D. (2010) *Protein Eng. Des. Sel.*, **24**, 3–9. doi:10.1093/protein/gzq097.

Lipovšek,D., Lippow,S.M., Hackel,B.J., Gregson,M.W., Cheng,P., Kapila,A. and Wittrup,K.D. (2007) *J. Mol. Biol.*, **368**, 1024–1041. doi:10.1016/j.jmb.2007.02.029.

Main,A.L., Harvey,T.S., Baron,M., Boyd,J. and Campbell,I.D. (1992) *Cell*, **71**, 671–678.

Mamluk,R., Carvajal,I.M., Morse,B.A. *et al.* (2010) *MAbs*, **2**, 199–208.

Martin-Killias,P., Stefan,N., Rothschild,S., Pluckthun,A. and Zangemeister-Wittke,U. (2011) *Clin. Cancer Res.*, **17**, 100–110. doi:10.1158/1078-0432.CCR-10-1303.

Mitchell,T., Chao,G., Sitkoff,D. *et al.* (2014) *J. Pharmacol. Exp. Ther.*, **350**, 412–424. doi:10.1124/jpet.114.214221.

Murray,B.C., Peterson,M.T. and Fecik,R.A. (2015) *Nat. Prod. Rep.*, **32**, 654–662. doi:10.1039/c4np00036f.

Patterson,A.W., Peltier,H.M. and Ellman,J.A. (2008) *J. Org. Chem.*, **73**, 4362–4369. doi:10.1021/jo800384x.

Polakis,P. (2015) *Pharmacol. Rev.*, **68**, 3–19. doi:10.1124/pr.114.009373.

Roman,J., Qiu,J., Dornadula,G., Hamuro,L., Bakhtiar,R. and Verch,T. (2011) *J. Pharmacol. Toxicol. Methods*, **63**, 227–235. doi:10.1016/j.vascn.2010.12.002.

Saber,H. and Leighton,J.K. (2015) *Regul. Toxicol. Pharmacol.*, **71**, 444–452. doi:10.1016/j.yrtph.2015.01.014.

Schmidt,M.M. and Wittrup,K.D. (2009) *Mol. Cancer Ther.*, **8**, 2861–2871. doi:10.1158/1535-7163.MCT-09-0195.

Serwotka-Suszczak,A.M., Sochaj-Gregorczyk,A.M., Pieczykolan,J., Krowarsch,D., Jelen,F. and Otlewski,J. (2017) *Int. J. Mol. Sci.*, **18**. doi:10.3390/ijms18020401.

Sievers,E.L. and Senter,P.D. (2013) *Annu. Rev. Med.*, **64**, 15–29. doi:10.1146/annurev-med-050311-201823.

Simon,M., Frey,R., Zangemeister-Wittke,U. and Pluckthun,A. (2013) *Bioconjug. Chem.*, **24**, 1955–1966. doi:10.1021/bc4004102.

Simon,M., Stefan,N., Borsig,L., Pluckthun,A. and Zangemeister-Wittke,U. (2014) *Mol. Cancer Ther.*, **13**, 375–385. doi:10.1158/1535-7163.MCT-13-0523.

Sochaj-Gregorczyk,A.M., Ludzia,P., Kozdrowska,E., Jakimowicz,P., Sokolowska-Wedzina,A. and Otlewski,J. (2017) *Int. J. Mol. Sci.*, **18**. doi:10.3390/ijms18081688.

Sochaj-Gregorczyk,A.M., Serwotka-Suszczak,A.M. and Otlewski,J. (2016) *J. Immunother.*, **39**, 223–232. doi:10.1097/CJI.0000000000000125.

Sokolova,E.A., Proshkina,G.M., Kutova,O.M., Balalaeva,I.V. and Deyev,S.M. (2017) *Acta Nat.*, **9**, 103–107.

Steinmetz,H., Glaser,N., Herdtweck,E., Sasse,F., Reichenbach,H. and Hofle,G. (2004) *Angew. Chem. Int. Ed Engl.*, **43**, 4888–4892. doi:10.1002/anie.200460147.

Strebhardt,K. and Ullrich,A. (2008) *Nat. Rev. Cancer*, **8**, 473–480. doi:10.1038/nrc2394.

Strop,P., Delaria,K., Foletti,D. *et al.* (2015) *Nat. Biotechnol.*, **33**, 694–696. doi:10.1038/nbt.3274.

Strop,P., Liu,S.-H., Dorywalska,M. *et al.* (2013) *Chem. Biol.*, **20**, 161–167. doi:10.1016/j.chembiol.2013.01.010.

Tolcher,A.W., Sweeney,C.J., Papadopoulos,K. *et al.* (2011) *Clin. Cancer Res.*, **17**, 363–371. doi:10.1158/1078-0432.CCR-10-1411.

Ullberg,S. (1954) *Acta Radiol. Suppl.*, **118**, 1–110.

Ullman-Cullere,M.H. and Charmaine,J.F. (1999) *Lab. Anim. Sci.*, **49**, 319–323.

Verma,S., Miles,D., Gianni,L. *et al.* (2012) *N. Engl. J. Med.*, **367**, 1783–1791. doi:10.1056/NEJMoa1209124.

Wakankar,A.A. and Borchardt,R.T. (2006) *J. Pharm. Sci.*, **95**, 2321–2336. doi:10.1002/jps.20740.

Walles,M., Rudolph,B., Wolf,T. *et al.* (2016) *Drug Metab.Dispos.*, **44**, 897–910. doi:10.1124/dmd.115.069021.

Xu,L., Aha,P., Gu,K. *et al.* (2003) *Chem. Biol.*, **10**, 91–92. doi:10.1016/s1074-5521(03)00004-8.

Younes,A., Bartlett,N.L., Leonard,J.P., Kennedy,D.A., Lynch,C.M., Sievers,E. L. and Forero-Torres,A. (2010) *N. Engl. J. Med.*, **363**, 1812–1821. doi:10.1056/NEJMoa1002965.

Zahnd,C., Kawe,M., Stumpp,M.T. *et al.* (2010) *Cancer Res.*, **70**, 1595–1605. doi:10.1158/0008-5472.CAN-09-2724.

Zhu,A.X., Gold,P.J., El-Khoueiry,A.B., Abrams,T.A., Morikawa,H., Ohishi, N., Ohtomo,T. and Philip,P.A. (2013) *Clin. Cancer Res.*, **19**, 920–928. doi:10.1158/1078-0432.CCR-12-2616.